Title:

Target-agnostic identification of human antibodies to *Plasmodium falciparum* sexual forms reveals cross stage recognition of glutamate-rich repeats.

Author List:

Axelle Amen[1,2,*], Randy Yoo[3,4,*], Amanda Fabra-García[5,*], Judith Bolscher[6], William J.R. Stone[7], Isabelle Bally[1], Sebastián Dergan-Dylon[1], Iga Kucharska[3], Roos M. de Jong[5], Marloes de Bruijni[6], Teun Bousema[5], C. Richter King[8], Randall S. MacGill[8], Robert W. Sauerwein[6], Jean-Philippe Julien[3,4,9,#], Pascal Poignard[1,2,10,#], Matthijs M. Jore[5,#]

[1] CNRS, Univ. Grenoble Alpes, CEA, UMR5075, Institut de Biologie Structurale, 38042 Grenoble, France
[2] CHU Grenoble Alpes, 38000 Grenoble, France
[3] Program in Molecular Medicine, The Hospital for Sick Children Research Institute, Toronto, ON, Canada.
[4] Department of Biochemistry, University of Toronto, Toronto, ON, Canada.
[5] Department of Medical Microbiology, Radboudumc, Nijmegen, the Netherlands.
[6] TropIQ Health Sciences, Nijmegen, the Netherlands.
[7] Department of Immunology and Infection, London School of Hygiene and Tropical Medicine, London, United Kingdom.
[8] Center for Vaccine Innovation and Access, PATH, Washington, DC 20001, USA
[9] Department of Immunology, University of Toronto, Toronto, ON, Canada.
[10] Department of Immunology and Microbiology, The Scripps Research Institute, La Jolla, CA 92037, USA.

*contributed equally
#contributed equally and corresponding authors:
Jean-Philippe.Julien@sickkids.ca; Pascal.Poignard@ibs.fr; Matthijs.Jore@radboudumc.nl

Competing Interests Statement:

The authors declare to have no competing interests.

Author Contributions:

A.A., R.Y, A.F-G., J.B. T.B., C.R.K., R.S.M., R.W.S, J-P.J., P.P. and M.M.J. designed research; A.A., R.Y., A.F-G., J.B., W.J.R.S., I.B., S.D-D., I.K., R.M.d.J. and M.d.B. performed research; A.A., R.Y., A.F-G., J.B., W.J.R.S., I.B., S.D-D., I.K., R.M.d.J., M.d.B. R.W.S., J-P.J., P.P. and M.M.J. analyzed data. A.A., R.Y. J-P.J., P.P. and M.M.J. wrote the original draft. All authors reviewed the manuscript.

Abstract:

Circulating sexual stages of *Plasmodium falciparum (Pf)* can be transmitted from humans to mosquitoes, thereby furthering the spread of malaria in the population. It is well established that antibodies (Abs) can efficiently block parasite transmission. In search for naturally acquired Ab targets on sexual stages, we established an efficient method for target-agnostic single B cell activation followed by high-throughput selection of human monoclonal antibodies (mAbs) reactive to sexual stages of *Pf* in the form of gamete and gametocyte extract. We isolated mAbs reactive against a range of *Pf* proteins including well-established targets Pfs48/45 and Pfs230. One mAb, B1E11K, was cross-reactive to various proteins containing glutamate-rich repetitive elements expressed at different stages of the parasite life cycle. A crystal structure of two B1E11K Fab domains in complex with its main antigen, RESA, expressed on asexual blood stages, showed binding of B1E11K to a repeating epitope motif in a head-to-head conformation engaging in affinity-matured homotypic interactions. Thus, this mode of recognition of *Pf* proteins, previously described only for PfCSP, extends to other repeats expressed across various stages. The findings augment our understanding of immune-pathogen interactions to repeating elements of the *Plasmodium* parasite proteome and underscore the potential of the novel mAb identification method used to provide new insights into the natural humoral immune response against *Pf*.

Impact Statement:

A naturally acquired human monoclonal antibody recognizes proteins expressed at different stages of the *Plasmodium falciparum* lifecycle through affinity-matured homotypic interactions with glutamate-rich repeats

Introduction:

The eradication of malaria remains a global health priority. In 2021, 247 million people were diagnosed with malaria with over 619,000 people succumbing to the disease (1). Malaria is caused by *Plasmodium* parasites: unicellular eukaryotic protozoans that transmit to human hosts through an *Anopheles* mosquito vector. Although insecticide-treated nets and various antimalarial compounds have aided in controlling the spread and combating severe clinical complications of the disease, mosquito and parasite strains resistant to such interventions have emerged (2). Thus, there is an urgent need to develop other technologies to help combat the spread of malaria, and eventually, contribute to the eradication of the disease.

The development of a highly efficacious malaria vaccine has been challenging, owing to the complex life cycle of malaria-causing parasites. The life cycle of *Plasmodium spp.* can be categorized into three distinct stages: the pre-erythrocytic, asexual blood stage, and sexual stages. Each step features the parasite undergoing large-scale morphological changes accompanied by modifications in proteomic expression profiles – with several proteins being exclusively expressed in a single stage (3). Therefore, vaccine-mediated humoral responses must be robust enough to generate sufficiently high-quality Ab responses to eliminate the majority of parasites at the stage the vaccine targets. As a result, one approach to vaccine development has focused on targeting “bottlenecks” in the parasite's life cycle where the number of parasites is low (4) (5).

The pre-erythrocytic stage – following the transmission of sporozoites to humans by a bite from an infected mosquito – is a bottleneck targeted by the only two malaria vaccines recommended by the World Health Organization, RTS,S/AS01 and R21/Matrix-M (6) (7). The vaccines are based on the circumsporozoite protein (CSP) – an essential protein expressed at high density on the surface of the parasite during the pre-erythrocytic stage (8) (9) (10). In its central domain, the protein contains various four amino acid repeat motifs – the most predominant of those being NANP repeats. Protective Abs elicited against CSP primarily target this immunodominant repeat region. A large proportion of these Abs engage in homotypic interactions which are characterized by direct interactions between two antibodies’ variable regions when bound to adjacent repetitive epitopes (11) (12) (13) (14) (15) (16) (17) (18) (19). Such interactions have been demonstrated to augment B cell activation and contribute to shaping the humoral response to CSP (12). Although these first-generation malaria vaccines only induce short-lived efficacy in a subset of the at-risk population (20) , they will undoubtedly assist in lowering the overall incidence of malaria in young infants with clear initial impact (21). Modeling suggests that for improvements towards eradication of the disease, combining multiple types of interventions that target different stages of the *Plasmodium* life cycle may strongly increase the efficacy of weaker interventions (22).

Another bottleneck in the parasite’s life cycle occurs during its sexual stage, which takes place in the mosquito vector. This stage begins when intraerythrocytic *Plasmodium* gametocytes (GCT), which are capable of eliciting antibody responses through clearance in the spleen (23), are taken up through a mosquito bloodmeal. Once inside the mosquito midgut, GCTs emerge from erythrocytes and mature into gametes (GMT) which then undergo fertilization ultimately resulting in the generation of sporozoites that can go on to infect the next human host. Vaccines that aim to target this life cycle bottleneck are known as transmission-blocking vaccines (TBVs) (24). The goal of TBVs is to elicit Abs that target sexual stage antigens to block the reproduction of the parasite in the mosquito and thus onward transmission to humans. Current TBV development efforts are primarily focused on two antigens, Pfs230 and Pfs48/45, as they are the targets of the most potent transmission-blocking Abs identified to date (25) (26) (27) (28). Indeed, individuals with sera enriched in Abs that target Pfs230 and Pfs48/45 were found to have high transmission-

reducing activity (29). Protective responses to Pfs230 and Pfs48/45 are well characterized at a molecular and structural level (26) (27) (28) (30) (31) (32) (33) (34). However, sera depleted in Abs targeting the pro domain and domain 1 of Pfs230 and domains 2 and 3 of Pfs48/45 can retain transmission-reducing activity while maintaining the ability to recognize the surface of parasites lacking Pfs48/45 and Pfs230 surface expression (29). This highlights the importance of expanding our understanding of Ab responses to other sexual stage antigens.

We designed a workflow for the isolation of Abs to sexual stage specific antigens from a donor who was repeatedly exposed to malaria parasites. Our efforts yielded a panel of 14 mAbs targeting Pfs230 and Pfs48/45 as well as other unidentified proteins, some with transmission-reducing activity. One mAb exhibited cross-reactivity to multiple antigens present at various stages of the parasite's life cycle, by targeting glutamate-rich repeats and engaging in homotypic interactions. This latest result underscores a pivotal role of repetitive elements in shaping the humoral response to *Pf.*

Results:

Agnostic memory B cell (MBC) sorting and activation identifies potential *Pf* sexual stage protein-specific mAbs.

We selected donor A, a 69-year-old Dutch expatriate who resided in Central Africa for approximately 30 years and whose serum was shown to strongly reduce *Pf* transmission, to isolate sexual stage-specific mAbs. We previously demonstrated the serum of this donor, donor A, largely retained its transmission-reducing activity (TRA) when depleted of Abs directed against the main transmission-blocking epitopes of Pfs48/45 and *Pf*s230 (29), suggesting the presence of Abs targeting other epitopes on these 2 proteins or directed at other proteins also involved in transmission.

PBMCs from the donor were thawed and a total of 1496 IgG+ memory B cells were sorted in 384-well plates **(Fig. 1) (Fig. S1A)**. Upon activation, single cell culture supernatants potentially containing secreted IgGs were screened in a high-throughput 384-well ELISA for their reactivity against a crude *Pf* gamete lysate, as well as against a gametocyte lysate for part of the sorted cells **(Fig. S1B and S1C)**. In total, supernatants from 84 wells reacted with gamete and/or gametocyte lysate proteins, representing 5.6% of the total memory B cells. Out of the 21 supernatants that were found positive after screening on both gamete and gametocyte lysates, six recognized both, while nine appeared to recognize exclusively gamete proteins, and six exclusively gametocyte proteins**.**

To isolate the corresponding mAbs, single B cell lysates from the 84 ELISA-positive wells were subjected to single B cell RT-PCR for immunoglobulin variable genes amplification. Following amplification and cloning, 14 mAbs, from 11 wells, were expressed as full human IgG1s **(Table S1) (Dataset S1).** Among the panel of mAbs, six used a kappa light chain (42%) and eight utilized a lambda light chain (57%). In three cases, both kappa and lambda sequences were retrieved from the same well, suggesting either the presence of two B cells or the expression of both chains in a single B cell (34).

Isolated mAbs exhibit distinct patterns of recognition of gamete surface proteins.

The 14 mAbs were first tested for binding to *Pf* sexual stage surface antigens in SIFA using wild-type and Pfs48/45 knock-out gametes **(Fig. 2A)**. Seven mAbs exhibited binding to approximatively half or more of gametes when tested at a concentration of 100 µg/ml. Among

these, four mAbs, B1C5K, B1C5L, B2C10L and B2E9L, recognized wild-type gametes with high scores (>68%) even at concentrations as low as 1 µg/ml. The binding of the B1C5K, B1C5L, B2C10L and B2E9L mAbs strongly decreased when using gametes that lacked surface-expressed Pfs48/45 and Pfs230, indicating that these four mAbs likely targeted one of these two antigens. Three other mAbs, B2D10L, B1C8L and B1E7K, displayed a similar recognition profile, albeit with notably smaller percentages of labeled wild-type gametes, particularly at the lower concentrations tested. This suggested a potential low affinity recognition of either Pfs48/45 or Pfs230 for these latter three mAbs.

Six of the remaining seven mAbs, B1C8K , B1D3L, B1D3K, B1F9K, B1C3L, and B2F7L, exhibited very weak or no binding in SIFA. For B1C8K, this showed that the light chain (kappa) did not correspond to the Ab that was originally selected in the screening process as the lambda version (B1C8L) exhibited strong binding. As for the other mAbs, the results indicated that they may be specific for proteins not expressed or only poorly expressed at the gamete surface.

Finally, one mAb, B1E11K, exhibited a distinctive binding profile in SIFA, recognizing only a fraction (approximately a third to a fifth) of the wild-type and Pfs48/45 knock-out gametes across all tested concentrations, suggesting potential binding to non-Pfs48/45 and Pfs230 proteins.

Isolated mAbs have varying transmission-reducing activities and recognize different *Pf* sexual stage proteins.

We were interested in investigating potential TRA for all identified mAbs. To do this, a standard membrane feeding assay (SMFA) was conducted in the presence of the isolated mAbs, revealing a range of transmission-reducing activities **(Fig. 2B)**. Overall, seven mAbs were confirmed to strongly reduce transmission (TRA > 80%) when tested at 500 µg/ml: B1C5K, B1C5L, B2C10L, B2E9L, B1C8L, B1D3L and B1F9K. Of those, two mAbs, B1C8L and B2C10L retained >50% TRA at a lower concentration (100 µg/ml). Notably, despite not showing recognition in SIFA, B1F9K and B1D3L displayed TRA – although only at high concentrations. Conversely, three mAbs exhibiting binding in SIFA, B2D10L, B1E7K and B1E11K, showed no activity in SMFA.

To gain deeper insight into the specificity of the various isolated mAbs, regardless of their transmission-reducing activity, we conducted further characterization via Western blot analyses using gametocyte extracts **(Fig. 2C)**. The B1C5K and B1C5L mAbs recognized a protein with a molecular weight matching that of Pfs48/45. This result was consistent with the findings from SIFA, providing further validation of the specificity of the B1C5K and B1C5L mAbs in targeting Pfs48/45. The B2C10L mAb displayed pattern of recognition that corresponded to Pfs230, similar to the anti-Pfs230 control mAb RUPA-96 (26). Once again, these results were in agreement with the findings from SIFA confirming the specificity of the B2C10L mAb in targeting Pfs230. The B1E11K mAb also appeared to bind to Pfs230 on the Western blot. However, in contrast to the RUPA-96 mAb, B1E11K only recognized the higher molecular band corresponding to Pfs230, suggesting exclusive recognition of the unprocessed form of this protein (35). Interestingly, besides Pfs230, BE11K also recognized several unidentified proteins ranging from 70 and 250 kDa with various intensities. These findings were consistent with the SIFA results, that also suggested potential recognition by B1E11K of proteins other than Pfs48/45 and Pfs230. Finally, all the other mAbs showed no clear binding to any protein from the gametocyte extract on the Western blot. In the case of those demonstrating binding in SIFA (B2E9L, B2D10L, B1C8L, B1E7K), this may be attributed to their recognition of conformational epitopes that are lost during Western blotting preparation, or possibly of specific recognition of proteins expressed in gametes but not gametocytes.

The recognition of Pfs48/45 by the B1C5K and B1C5L mAbs was subsequently confirmed through an ELISA using full-length recombinant Pfs48/45 **(Fig. 2D)**. Notably, none of the other mAbs of the panel displayed binding to this Pfs48/45 recombinant protein construct. To further pinpoint the domain targeted by B1C5K and B1C5L, an ELISA was performed using constructs corresponding to domains 1-2, 2-3 and 3 revealing that these two mAbs targeted Domain 2 of Pfs48/45 **(Fig. 2E)**. This is in agreement with prior work indicating mAbs to Domain 2 of Pfs48/45 are generally mAbs with low potency (27).

The combined findings above strongly pointed to Pfs230 as the target of mAb B2C10L. We thus tested this mAb in ELISA for binding to the Pfs230CMB construct (D1-harbouring construct) (36) No reactivity was observed **(Fig. 2F)** suggesting that B2C10L may recognize other Pfs230 domains than the one tested, or recognize epitopes not properly displayed in the construct used.

In summary, our target-agnostic mAb isolation approach successfully identified mAbs against *Pf* sexual stage proteins, some of which exhibited TRA and some of which target Pfs48/45 or Pfs230. However, given that the mAbs isolated in this study showed substantially lower TRA than mAbs identified previously (37) (38) we elected not to investigate them further. Instead, we were intrigued by the binding properties of B1E11K, which showed cross-reactivity with various *Pf* proteins, including Pfs230. Such cross-reactivity has been shown as a hallmark of the human Ab response to *Pf* and explored at the serum level but to our knowledge has never been studied at the mAb level (39) (40). Thus, we rationalized a more detailed molecular characterization of this mAb may provide insights into this relatively unexplored phenomenon.

The B1E11K mAb cross-reacts to distinct sexual and asexual stage *Pf* proteins containing glutamate-rich repeats.

First, to ensure the ability of B1E11K to recognize different proteins in Western blotting experiments was not due to polyreactivity, the mAb was tested in ELISA against a panel of human proteins, ssDNA and LPS. The 4E10 mAb, a well-known anti-HIV gp41 polyreactive mAb (41), was used as a positive control. The B1E11K mAb did not bind any of the antigens on the panel at any significant level, even at a high 50 µg/ml concentration, and therefore polyreactivity was ruled out **(Fig. S2A)**.

To identify antigens recognized by B1E11K, immunoprecipitation experiments were conducted using gametocyte extract. Proteins of different molecular weights were specifically detected in the B1E11K immunoprecipitate but not when using the anti-HIV control mAb **(Fig. S2B)**. Mass spectrometry analysis of the corresponding gel slices revealed recognition of Pfs230, confirming the Western blot results.

The specificity of B1E11K was further tested using a protein microarray featuring recombinant proteins corresponding to putative antigens expressed at the sexual stage as well as proteins expressed at different stages of the *Pf* life cycle (29)**.** The results showed that B1E11K exhibited high level reactivity (>8-fold higher than the negative control, minimum signal intensity rank 15th of 943 array targets)against several antigens, some expressed at the sexual stage (*i.e.* Pf11.1), others at the asexual stage (*i.e.* LSA3, RESA, RESA3) (**Fig. 3A**). Analysis of the primary amino acid sequence of the antigens recognized in the array suggested homology in several cases, based on the presence of glutamate-rich regions **(Fig. S3)**. To analyze the numerous repeated motifs contained in these proteins, we used the RADAR (Rapid Automatic Detection and Alignment of Repeats) software (42). Although B1E11K recognition of Pfs230 fragments on the array was lower than our cut off for further analysis (3.4-fold higher than the negative control, maximum signal intensity rank 30th of 943 array targets), its sequence was also analyzed using

RADAR due to its recognition by B1E11K in the immunoprecipitation experiments (**Fig. S4**). The analysis showed Pfs230 and several of the proteins recognized by B1E11K on the array contained diverse patterns of glutamate-rich repeats of different lengths and compositions. Among these proteins, Pfs230, Pf11.1, RESA, RESA3 and LSA3 presented the most similar glutamate repeats, following an "EE-XX-EE" pattern **(Fig. S4)**. Pfs230 contains adjacent EE-VG-EE repeats which are located in the domain of the protein which is cleaved upon gametocyte egress from erythrocytes (43). RESA and RESA3 contain 20 and nine EE-NV-EE overlapping repeats at the C terminus of the protein, respectively. LSA3 contains two overlapping EE-NV-EE repeats. Finally, 221 non-adjacent EE-LV-EE repeats span the whole Pf11.1 megadalton protein.

To verify the recognition of the aforementioned proteins, a Western blot was performed with recombinant forms of RESA, RESA3, LSA3, and of a Pf11.1 domain (44) **(Fig. 3B)**. Domain 1 of Pfs230, which does not contain the EE-VG-EE repeats, was also included. The results confirmed the binding of B1E11K to all the proteins tested except for Pfs230D1, as expected. Overall, the data showed that the B1E11K mAb recognizes various *Pf* proteins from different stages, all containing glutamate-rich repeats.

To validate the B1E11K mAb specifically targets glutamate-rich repeats, we synthesized five biotinylated peptides derived from the various repeats found in the proteins identified above to test for binding in sandwich ELISA experiments **(Fig. 3C)**. Overall, the B1E11K mAb bound to all peptides **(Fig. 3D)**. However, it exhibited a higher specificity for the RESA-derived peptides with an EC_{50} at least 100 times greater compared to EC_{50} values obtained with the other glutamate-rich peptides. Altogether, this suggests the main antigenic targets of B1E11K are RESA and RESA3, which contain the EENV repeats.

Since B1E11K bound to RESA-based peptides the strongest, we synthesized shorter RESA peptides for a more precise determination of the B1E11K minimal sequence epitope **(Fig. 4A)**. When tested on the RESA peptide panel, B1E11K mAb binding to RESA P2 (16AA) and RESA 14AA, 12AA, and 10AA was similar, all exhibiting close EC_{50} values **(Fig. 4B)**. No binding was observed for the 8AA RESA peptide, suggesting the 10AA peptide contained the minimal epitope. We hypothesized the similar EC_{50} values may be a result of avidity effects and thus, we performed the same experiment with recombinant B1E11K Fab **(Fig. 4C)**. Although B1E11K Fab bound both RESA P2 (16AA) and RESA 14AA peptides with comparable strength of binding, both RESA 12AA and RESA 10AA peptides displayed comparatively poorer EC_{50} values with the RESA 10AA peptide displaying the lowest detectable binding strength. The binding affinity and kinetics of the interaction was also determined through biolayer interferometry (BLI). We performed experiments using the minimal sequence required for binding determined through ELISA [RESA 10AA peptide and the RESA P2 peptide (16AA)]. When immobilizing the peptide to the sensors, an approximately six-fold difference in affinity between the 10AA peptide (K_D = 484 nM) **(Fig. 4D)** and the P2 peptide (16AA) (K_D = 74 nM) **(Fig. 4E)** was observed.

Four EENV repeats permit two B1E11K Fabs to bind.

Given the repetitive nature of the antigenic targets of B1E11K and differences in binding events captured in our BLI experiments, we hypothesized that more than one B1E11K Fab could potentially bind to the longer, RESA P2 (16AA) peptide. Thus, we performed isothermal titration calorimetry using the same two RESA peptides as in the BLI experiments to determine the binding stoichiometries. We observed when titrating the B1E11K Fab into RESA 10AA, a binding stoichiometry of N = 1.0 ± 0.2 **(Fig. 4F and Table 1)**. When using the RESA P2 (16AA) peptide, a stoichiometry of N = 2.0 ± 0.1 was observed **(Fig. 4G and Table 1)**. To further corroborate our binding stoichiometry findings, we performed size-exclusion chromatography coupled with multi-

angle light scattering (SEC-MALS) to determine the molecular weight of the 2:1 Fab:peptide complex **(Fig. 4H)**. We incubated a molar excess Fab:peptide (6:1) sample to saturate all B1E11K Fab binding sites present on the RESA peptide to obtain a solution containing the putative complex and excess monomeric Fab. The resulting chromatogram revealed two species eluted from the column. The molecular weight of the heavier species was in line with what would be expected from a 2:1 Fab:peptide complex (92 kDa) in which the mass determined fell within the range of experimental error. A negative-stain electron microscopy (nsEM) map reconstruction of the 2:1 Fab:peptide complex recovered from the SEC-MALS experiment **(Fig. 4H)** permitted the fitting of two Fab molecules, further supporting the 2:1 binding model **(Fig. 4I)**.

B1E11K binds EENV repeats in a head-to-head conformation leveraging homotypic interactions.

To obtain a full structural understanding of the observed repeat cross-reactivity and selectivity for RESA exhibited by B1E11K, we solved a 2.6 Å structure of the B1E11K:RESA P2 (16AA) peptide complex **(Fig. 5A and Table 2)(Dataset 2)**. The electron density at the binding interface is unambiguous and included density for the entirety of the repeat region of the peptide **(Fig. S5).** Looking at the binding interface between the two Fabs and peptide reveals the structural basis for cross-reactivity **(Table 1, Fig. S6 and Table S2)**. The paratope of B1E11K is highly enriched in arginine and histidine residues giving rise to a highly electropositive groove **(Fig. 5B)**. These residues form a plethora of salt-bridging interactions with the glutamate residue side chains of RESA repeats **(Fig. 5C)**. These interactions are supplemented by hydrogen bonding interactions of backbone serine and glycine residues of the B1E11K paratope as well as a hydrogen bond involving W33 found in the heavy chain of Fab B. Multiple hydrogen bonding interactions are made with B1E11K through the side chains of the asparagine residues of RESA repeats (EENV) **(Fig. 5D)** that would not exist in the context of binding to the repeats of Pf11.1 (EELV or EEVIP or EEFIP or EEVVP) or Pfs230 (EEVG) **(Fig. 3C),** as these residues lack side chains that can form hydrogen bonds. This likely leads to the observed higher specificity of B1E11K for RESA repeats demonstrated in our ELISA experiments **(Fig. 3D)**.

Additionally, the crystal structure of the antibody-antigen complex revealed the presence of homotypic antibody-antibody contacts, through two interfaces surrounding the repeat peptide binding groove **(Fig. 5E) (Fig. S7 and Table S3)**. The first interface features a salt-bridging network involving D60 of the Fab B kappa chain forming two salt bridges with R52 and H52A of the Fab A HCDR2 **(Fig. 5F)**. Additionally, R54 of the Fab A HCDR2 forms two hydrogen bonds and a salt bridge with the Fab B kappa chain side chains of S55 and E56. Finally, Y58 of the Fab B HCDR2 forms a hydrogen bond with the side chain of S53 of the Fab A HCDR2. The second interface is less extensive featuring two hydrogen bonds between Y32 and S31 of the Fab B HCDR1 and the Fab A KCDR1 T29 and R27, respectively **(Fig. 5G)**.

Analysis of the B1E11K sequences with IgBLAST (45) reveals B1E11K heavy and light chain have high similarity to the IGHV3-7 and IGKV3-20 germline sequences **(Fig. S8)**. This analysis also indicates multiple residues involved in the homotypic interaction interface have undergone somatic hypermutation. Residues of the CDR2 heavy chain of Fab A, R52 and H52A, and kappa chain CDR1 residues of Fab B, T29 and R27, form various electrostatic and van der Waals interactions which are mutated from the inferred germline sequences **(Fig. 5F and 5G, Fig. S7-8)**. In summary, our biophysical and structural characterization revealed the basis of cross-reactivity and specificity to RESA repeats (EENV) through a binding interface highly electrostatic in nature, featuring affinity-matured homotypic interactions between adjacent antibody molecules when in its antigen-bound state.

Discussion:

Here, we introduce an innovative strategy that circumvents the use of recombinant proteins, to explore humoral immunity to *Pf* sexual proteins. We used target-agnostic MBC sorting and activation, followed by screening to assess reactivity against *P. falciparum* gamete lysate and, for a fraction of the sorted cells, gametocyte lysate. The approach enabled the identification of a panel of mAbs targeting diverse *Pf* proteins, including some that exhibit transmission reducing activity. The total number of isolated Abs was relatively low due to the limited number of cells used. However, the identified B cells accounted for 5.6% of the total number, which suggest that there is a relatively high proportion of B cells specific for gamete proteins in the memory compartment of this donor, considering not all B cells were activated (typically 70-80 % activation in our experiments). Furthermore, despite screening with a parasite extract containing a mixture of intracellular and surface proteins, half of the mAbs displayed binding to gametes in SIFA, and/or exhibited TRA. This suggests Ab responses to surface proteins and proteins involved in transmission were high in this particular donor, potentially explaining the potent TRA observed with the serum.

Among the seven mAbs exhibiting TRA, three were found to recognize the well-defined TRA targets Pfs48/45 and Pfs230. The B1C5L and B1C5K mAbs were shown to recognize Domain 2 of Pfs48/45 and exhibited moderate potency, as previously described for Abs with such specificity (27). These 2 mAbs were isolated from the same well and shared the same heavy chain; their similar characteristics thus suggest that their binding is primarily mediated by the heavy chain. Furthermore, a mAb identical to B1C5K was recently isolated from the same donor using a single B cell selection approach with recombinant Pfs48/45 (27). Pfs230 was shown, via SIFA and Western blot, to be targeted by the B2C10L mAb, which failed to bind the D1 domain in ELISA. This confirms TRA may be mediated through binding to domains other than D1, the current main vaccine candidate (46).

The remaining four mAbs exhibiting TRA did not clearly demonstrate recognition of either Pfs230 or Pfs48/45. Among those mAbs, B2E9L, and to a lesser extent B1C8L, showed recognition of WT gametes but not Pfs48/45 KO gametes in SIFA. However, Western blot did not identify any protein targeted by these two mAbs and they did not bind to Pfs48/45 in ELISA. Therefore, we hypothesize these two mAbs target a protein associated with the Pfs48/45-Pfs230 complex, which is absent in Pfs48/45 KO gametes (47). An alternative explanation for the antigenicity of B2E9L and B1C8L is that these two mAbs may target a Pfs230 conformational epitope that is not represented in Western blot assays. The last two mAbs that exhibited TRA, B1D3L and B1F9K, displayed no reactivity in SIFA, neither on WT nor KO gametes, and did not show any recognition in Western blot. In the case of B1D3L, the selection during screening was based on recognition of the gametocyte lysate while testing on the gamete extract was negative. This mAb may possibly target a protein only expressed on gametocytes (indicating that the epitope might be conformational and not properly displayed in Western blotting with gametocyte extract). Regarding B1F9K, it is somewhat surprising that this mAb, which was originally selected based on positivity in the gamete extract ELISA, did not display reactivity in SIFA while still exhibiting TRA. Further exploration is needed to understand this apparent discrepancy. Overall, these latter mAbs, which do not recognize well-defined TRA targets, demonstrated lower potency in the SMFA assay compared to some of the best characterized mAbs with such activity. Nevertheless, they could still be of strong interest in defining potential novel TRA targets, and further investigations are needed.

Seven of the fourteen mAbs isolated did not exhibit TRA. Of those, four exhibited some level of binding in SIFA: B1E11K, B2D10L, B1E7K and B2F7L (albeit very weakly). This may suggest either the recognition of proteins involved in transmission but with an insufficient affinity to exert a significant effect, recognition of non-functional epitopes in proteins that play a role in transmission, or the recognition of proteins unrelated to the transmission process altogether.

B1E11K recognized various proteins from both the Pf sexual stage and asexual stages, all containing glutamate-rich repeats. Repetitive regions rich in glutamate residues have been previously found to be highly immunogenic in malaria-experienced individuals. A study investigating Ab responses against asexual stage antigens of *Pf* associated with erythrocyte invasion using sera from individuals from various cohorts found that the repetitive regions rich in glutamate residues within these antigens were predominantly recognized (39). Another investigation into sera from individuals from Uganda corroborated this finding (40). Raghavan et al noted the Abs that target these repeats may be potentially cross-reactive but emphasized that such a claim could only be demonstrated by direct investigations into mAbs. To our knowledge, only four mAbs that target glutamate-rich repeats have been described in which their epitopes have been determined. Of those mAbs, three were obtained following mouse immunization, and only one was of human origin. The murine mAbs 1A1 (48) and 1E10 (49) recognize Pf11.1-derived repeat peptides ([PEE(L/V)VEEV(I/V)]$_2$); the murine mAb 9B11 (50) is able to bind to a peptide containing four EENV repeats of RESA; and finally the human mAb 33G2 (51) is specific for a peptide repeat sequence found in Ag332 (VTEEI) (52). Despite all targeting linear epitopes containing tandem glutamate residues (EE), only 33G2 appeared to exhibit cross-reactivity (53) and none had been structurally characterized. Thus, our structure provides critical insights into how glutamate-rich-repeat targeting Abs from immune individuals can cross-react with various *Pf* proteins expressed at different life cycle stages.

A most revealing observation from our structure is the presence of affinity-matured antibody-antibody homotypic interactions in the context of recognizing repetitive tandem glutamate residues present across the *Pf* proteome. The finding that B1E11K targets a repetitive epitope whilst engaging in affinity-matured homotypic interactions is similar to how Abs elicited against repetitive elements of CSP can also bind through homotypic interactions (12) (14) (15) (13) (16) (19) (54) (17) (18) (11). We have previously shown that B cells expressing B cell receptors (BCRs) interacting via homotypic interactions activate more robustly in comparison to B cells that have mutated BCRs that disrupt this interaction (12). This strong B cell activation, presumably mediated through the cross-linking of multiple BCRs at the B cell surface (55), has been suggested to limit affinity maturation in germinal centers, potentially due to early exit of B cells, favouring the elicitation of short-term low-affinity Abs to CSP over durable high-affinity responses, thus leading to suboptimal protective responses (56). However, this phenomenon may potentially be altered with the development of cross-reactive responses against repeats of slightly different content (57) (58) (59). Whether such insights extend to other anti-repeats Ab responses in general and anti-glutamate rich repeats in particular remains largely unexplored.

Our observation of the recognition of RESA glutamate repeats by the B1E11K mAb through homotypic interactions tends to confirm a generalizable property of B cell responses to repetitive antigens where Abs can bind in close proximity. Here, we observed that B1E11K mAb exhibits a fair degree of somatic hypermutation and a relatively high affinity for RESA and cross-reactivity to other antigens. This finding provides further credence to the proposition that high affinity matured Abs to repeats can be elicited when cross-reacting to motifs of slightly different content, in the present case derived from antigens expressed at different stages of the *Pf* life cycle. Nonetheless, cross-binding to repeats-sharing proteins from different stages, as demonstrated with the B1E11K mAb, could also represent another mechanism by which repeated motifs may

impact protective responses. Indeed, Abs elicited by one protein with repeats may hinder subsequent potential protective responses to cross-recognized proteins expressed later in the parasite life cycle through antibody feedback mechanisms such as epitope masking (40) (60) (61) (62).

Ultimately, understanding the dynamics of how the immune system responds to repetitive elements could be critical for the future rational design of malaria vaccines. A desired characteristic for next-generation malaria vaccines will be the ability to elicit Abs that can inhibit at multiple stages of the parasite's life cycle to prevent infection, reduce clinical manifestations, and lower the spread of the disease (63) (64). This could be accomplished by designing a multi-stage malaria vaccine that displays antigens expressed at various points of the parasite's life cycle. Utilizing glutamate-rich repeats in such a design may present benefits as a single antigen could potentially give rise to sera which contain Abs that can both lower the clinical burden (asexual stage-targeting Abs) and transmission of the disease (sexual stage-targeting Abs). Indeed, Abs elicited against the repetitive elements described here have been demonstrated to be associated with a lower incidence of disease (65) (66) (67) as well as disrupt the maturation of sexual stage parasites (48) in *in vitro* assays – although we note that mAb B1E11K isolated and characterized in this study did not show TRA.

As such, future work will be necessary to better understand the structure-activity relationships of mAbs targeting *Pf* repetitive elements across life cycle stages, such as the glutamate-rich repeats, and validate these targets as viable for next-generation malaria vaccines seeking the induction of long-lived immunity. The high-throughput target-agnostic approach used here has a strong potential for a further comprehensive exploration of humoral immunity to *Pf*.

Material and methods:

PBMC sampling.

Sampling of donor A PBMCs was conducted following ethical guidelines described in (29). Donor A had lived in Central Africa for approximately 30 years and reported multiple malaria infections. Donor A had recently returned to the Netherlands and had a malaria infection at the time of sampling, but gametocyte prevalence and density were not recorded.

Preparation of MBCs culture plates.

Plates were prepared the day ahead of sorting and incubated at 37 °C. Three-hundred-eighty-four-well cell culture plates (Corning #CLS3570-50EA) were prepared with the appropriate memory B cell stimulation media one day before cell sorting, to allow the feeder cells sedimentation at the bottom of the wells. Iscove's Modified Dulbecco's Medium (IMDM) (Gibco #12440061) was complemented with 1% penicillin-streptomycin (Thermo Fisher Scientific #10378016) and supplemented with 20% FBS (Gibco #16170-078). A cytokine cocktail was added to stimulate MBCs activation, with IL21 (Preprotech #200-21) at 100 ng/ml and IL2 (Preprotech#200-02) at 51 ng/ml. Fibroblasts expressing CD40L "L cells" (68) were irradiated at 50 Gy and 5000 were added in each well as feeder cells.

MBCs sorting.

Cryopreserved PBMCs were thawed by a brief incubation in a 37 °C warm bath and stained with the following Miltenyi REA antibodies before sorting by flow cytometry: anti-CD3 (#130-114-519), anti-CD19 (#130-113-649), anti-CD20 (#130-113-649), anti-IgM (#130-113-476), anti-IgD (#130-110-643) and anti-IgA (#130-113-476). An Aqua LIVE/DEAD stain was also used (Thermo Fisher Scientific #L34957). Following staining, MBCs were sorted into the 384-well cell culture plates. After an 11 day culture period, supernatants were harvested using a pipetting robot (Eppendorf #5073) and transfered to storage plates (Greiner #788860-906). MBCs were lysed and their mRNA purified using the mRNA TurboCapture kit for 384 wells (Qiagen #72271). Lysates were stored at -80 °C. Lysates from selected wells were further transferred into 96-well RT-PCR plates (Biorad #HSP9641) to perform RT-PCR.

Gamete / gametocyte extract ELISA.

Gamete or gametocyte lysate were prepared as described (27). Three hundred eighty four well plates (Thermo Fisher Scientific #460372) were coated with 7500 lysed gametes / gametocytes per well. Plates were incubated at 4°C overnight, then wells were washed three times with PBS-Tween 0.05%, prior to 1 hour blocking (with a 1% BSA - 1% PBS-Tween 0.05% solution). Cell culture supernatants (diluted ½ in blocking solution) were dispensed into the wells for a 1-hour incubation step. Following washing, secondary antibody (Thermo Fisher Scientific #A18814) diluted at 1/2000 was added and incubated for 1 h. Plates were then washed and 15 µl of CDP-substrate (Thermo Fisher Scientific #T2146) was added. The reaction was measured using Biotek Synergy 2 reader. Positivity threshold was determined as the average background OD + (3 x SD (background OD)). TB31F (anti-Pfs48/45 mAb), and 2544 (anti-*Pf*s25 mAb) were used as positive controls, while 399 (anti-CSP mAb) was used as negative control.

Monoclonal antibody isolation and production.

Nested multiplexed PCRs were performed on single MBCs from selected wells following the protocol outlined by Tiller et al (36). PCR products were sent for sequencing (Genewiz®) and sequences analyzed for Ig gene features using the IMGT (ImMunoGeneTics) database (69). Ig gene family-specific primers were used for cloning, as described by Tiller et al (PMID: 17996249) (36). Purified PCR products were cloned into vectors encoding for either IgG1 lambda, kappa or heavy constant regions. For transient mAb expression and secretion, HEK293 F cells were co-transfected with plasmids coding the Ab heavy chain and the corresponding light chain using 293 Fectin (TF#12347500). A protein A-Sepharose column (Sigma #ge17-1279-03) was used for mAb purification. Elution of mAbs was conducted with 4.5 ml of glycine 0.1 M (pH 2.5) and 500 µl of Tris 1 M (pH 9). The purified mAbs were subsequently subjected to buffer exchange and concentration with AmiconUltra (Merck #36100101).

Fab production.

The DNA sequences of VK and VH of the B1E11K Fab domain were cloned upstream of human Igκ and Igγ1-CH1 domains respectively and inserted into a custom pcDNA3.4 expression vector. The plasmids were co-transfected into FreeStyle 293 F cells that were cultured in FreeStyle 293 Expression Media (Gibco #12338018) using Fectopro (Polyplus, 101000003). The recombinant Fab was purified via KappaSelect affinity chromatography (Cytiva #17545812) and cation exchange chromatography (MonoS, Cytiva 17516801).

Gamete surface immuno-fluorescence assay (SIFA).

To perform gametes SIFA, either WT or Pfs48/45 KO (70). *Pf* strains were used. Pfs48/45 KO also downregulates Pfs230 retention at the gamete's surface (71). Wild-type or Pfs48/45 KO gametes were obtained following gametocyte activation in FBS for 1 h at room temperature. Gametes were washed with PBS and incubated with mAbs dilutions in PBS containing 0.5% PBS and 0.05% NaN_3 (SIFA buffer) for 1 hr at 4 °C in sterile V bottom plates (VWR#736-0223). After incubation, wells were washed three times with SIFA buffer and secondary antibody Alexa Fluor® 488 Goat Anti-Mouse IgG (H+L) (Invitrogen#A11001) diluted 1/200 added for a 1-hour incubation step on ice. Following a washing step, gametes were suspended in 4% paraformaldehyde and transferred into 384-well clear bottom black plates. Four images per well were taken using the ImageXpress® Pico Cell Imaging System (Molecular Devices).

Western blot.

For western blots with gametocyte extract, *Pf* NF54 gametocyte extract was prepared as described above. The extract was mixed with NuPAGE™ LDS sample buffer (TF # NP0008) and heated for 15 min at 56 °C. A 25 mM dithiothreitol was added for samples reduction. The equivalent of 1 million lysed gametocytes was deposited per lane. A NuPAGE™ 4-12% Bis-Tris 2D-well gel (TF#NP0326BOX) was used for proteins separation. Using the Trans-Blot Turbo system (Bio-Rad #1704150) samples were then transferred to a 0.22 µm nitrocellulose membrane (Bio-Rad #1620150). The blots were cut into strips, blocked with 5% skimmed milk in PBS and incubated with 5 µg/ml of the mAb to be tested. Strips were incubated with the secondary anti-human IgG-HRP antibody (Pierce#31412), diluted 1/5000 in PBS-T. Clarity Western ECL substrate (Bio-Rad #1705060) was used for development and strips were imaged with the ImageQuant LAS4000 equipment (GE Healthcare).
For western blot with recombinant proteins, we used Pfs230CMB (amino acids 444-730) expressed in a plant-based transient expression system (72), and RESA3 (amino acids 570-1090), RESA (amino acids 66-585), LSA3 (amino acids 805-1558) and Pf11.1 (amino acids 3657-3734) that were expressed wheat germ cell free extract (https://repository.ubn.ru.nl/bitstream/handle/2066/289602/289602.pdf?sequence=1). All antigens contained a C-terminal His-tag. RESA and LSA3 also had an N-terminal GST-tag. The equivalent of 150 ng of protein was loaded per lane. An SDS 4-20% gel (BioRad # 4561094) was used for protein separation under non-reducing conditions. Further steps were performed following the protocol described above.

Recombinant Pfs48/45 and Pfs230 ELISA.

ELISAs with full length Pfs48/45 and fragments thereof, and Pfs230CMB were performed as previously described (27) (72). In short, Nunc MaxiSorp 96-wells plates (ThermoFisher) were coated with recombinant Pfs48/45 or Pfs230CMB proteins, blocked with 5% skimmed milk in PBS + 0.1% Tween-20 and washed. Plates were then incubated with 10 or 30 µg/mL mAb in 1% skimmed milk in PBS. After washing, plates were incubated with 1:60,000 Goat anti-Human IgG/HRP-conjugated antibody (Pierce, Cat. No. 31412) in 1% skimmed milk in PBS + 0.1% Tween-20. After washing, plates were developed with 3,3′,5,5′-Tetramethylbenzidine (TMB) and the reaction was stopped with H_2SO_4. Absorbance was measured at 450nm. mAbs were considered positive when the absorbance was higher than the mean absorbance plus three standard deviations of seven negative mAbs.

MAb poly-reactivity testing in ELISA.

The coating antigens were diluted to 1 µg/ml. Antigens used were: ssDNA (Sigma #D8899-5MG), disialoganglioside GD1α (Sigma #G2392-1MG), lipopolysaccharide (Sigma #L2630-10MG),

transferrin (Sigma #T3309-100MG), apotransferrin (Sigma #T1147-100MG), hemocyanin (Sigma #H7017-20MG), insulin (Sigma #I2643-25MG), cardiolipin (Sigma #C0563-10MG), albumin and histone (Sigma #H9250-100MG). Secondary antibody used was a phosphatase-coupled goat anti-human IgG (Jackson immuno #109 056 098). Optical densities were read at 405 nm, one hour after the addition of pNPP.

Standard Membrane Feeding Assay (SMFA).

SMFA experiments were performed using *Pf* NF54 wild-type gametocytes with oocyst count readout, following a protocol set up by Ponnudurai et al (73). Briefly, blood meals containing cultured gametocytes mixed with antibodies were fed to *A. stephensi* mosquitoes (Nijmegen colony). For each condition, 20 fully fed mosquitoes were analyzed. Reported antibody concentrations are concentrations in the total blood meal volume. mAbs that showed >80% transmission reducing activity (TRA), i.e. reduction in oocysts compared to a negative control, were tested in a second independent SMFA experiment. Transmission reducing activity (TRA) from one or two independent SMFA experiments was calculated using a negative binomial regression model as previously described (74). SMFA data analyses were done in R (version 4.1.2).

Microarray.

Microarray design and protocol have been extensively detailed in (29) and (75) . Briefly, selection proteins to be printed on the array was made on the basis of a systematic analyses of proteomic data by Meerstein-Kessel et al (76). In total 943 protein targets representing 528 unique gene IDs were expressed for the array using an in vitro transcription translation system; these were printed onto nitrocellulose coated slides at the University of California, Irvine as described previously (75). Microarray slides were rehydrated in blocking buffer (GVS #10485356) while B1E11K was diluted 1:100 in a 20% E. coli lysate/blocking buffer solution and incubated for 30 min. Blocking buffer was discarded and diluted B1E11K added to the array slides for incubation overnight at 4° C with continual rocking. Following three washes with TBS-Tween-20 0.05%, slides were probed with a fluorophore conjugated secondary antibody (Southern Biotech, Goat Anti-Human IgG-TXRD) at a concentration of 0.5 µg/mL (1:2000) in 2% E. coli lysate/blocking buffer solution. After three washes, slides were removed from their casettes and rinsed in ddH20air dried in a centrifuge and scanned using a GenePix 4300A High-resolution Microarray Scanner (Molecular Devices). Data treatment and analysis were performed using R (77). Correction for local array target spot background was done using the 'backgroundCorrect' function of the limma package (78). Background corrected values were log2 transformed and normalised to systematic effects by subtraction of the median signal intensity of the negative IVTT controls (internally within four subarrays per sample). The final normalised data are a log2 MFI ratio of target to control reactivity: a value of 0 represents equality with the vehicle control, and a value of 1 indicates a signal twice as high.

Immunoprecipitation.

Briefly, we used tosyl-activated beads (Invitrogen #14203) to covalently link B1E11K and incubated these beads with a gametocyte lysate to enable antigen capture. Immunoprecipitated antigens were eluted, and the elution fraction was run on an SDS-PAGE gel and silver-stained. A negative control immunoprecipitation experiment was performed using an anti-HIV gp120 mAb. As shown in **sup Fig 2B**, two bands with a molecular weight greater than 250 kDa, and a third one with a molecular weight around 55 kDa were specifically detected in the B1E11K immunoprecipitate, in comparison to the control antibody. The 3 bands were cut and sent for mass

spectrometry analysis. Data were analyzed by querying the entire proteome of *Plasmodium falciparum* (NF54 isolate) in the Uniprot database.

Peptide synthesis.

Peptides were produced by P. Verdié team, IBMM - SynBio3, Montpellier, France. Lyophilized peptides were solubilized in PBS.

ELISA with biotinylated peptides.

ELISA protocol was similar to the protocol described above. Briefly, 96-well ELISA plates were coated overnight at 4° C with 0.5 µg/ml of streptavidin (TF # 434301). Plates were washed and then blocked for 1 h. Following wash, peptides diluted at 0.5 µg/ml were added to the plates for a 1 h incubation. The plates were washed and serially diluted mAbs were added. mAb fixation was detected using phosphatase-coupled goat anti-human IgG (Jackson Immuno #109 056 098) and para-nitrophenylphosphate (Interchim #UP 664791). The enzymatic reaction was measured at 405 nm using a TECAN Spark 10M plate reader. Half maximal effective concentration (EC50) was calculated from raw data (O.D) after normalization using GraphPad Prism (version 9) “log agonist versus normalized response” function.

BioLayer Interferometry (BLI) assay.

All BLI experiments were performed using an Octet Red96e Instrument (PallForteBio), at 25°C and under 1000 rpm agitation. SAX biosensors (Sartorius # 18-5117) were pre-wetted in BLI Buffer [PBS (pH 7.4) + 0.01% (w/v) BSA + 0.002% (v/v) Tween-20] for 10 min. Biotinylated peptides were loaded onto the biosensors until the top concentration of B1E11K Fab utilized in kinetic assays (2500 nM for RESA 10 AA peptide and 625 nM for RESA P2 peptide) yielded a response value of ~ 1.2 nm. An association step was conducted by dipping the sensors into a titration series of ½ serially diluted B1E11K Fab for 30 seconds. The dissociation step was conducted by dipping the biosensors into BLI Buffer for 1200 seconds. Background subtractions were done using measurements where experiments were performed with biosensors treated in the same conditions but replacing Fab solution with BLI Buffer. Kinetic data were processed using the manufacturer's software (Data analysis HT v11.1).

Isothermal Titration Calorimetry.

An Auto-ITC200 (Malvern) was used to conduct calorimetric experiments. The RESA P2 peptide, RESA 10AA peptide, and recombinant B1E11K Fab were buffer-exchanged into Tris-buffered saline (20 mM Tris pH 7.0, and 150 mM NaCl). The B1E11K Fab was concentrated at 90 - 110 µM for experiments utilizing the RESA P2 peptide and 60 - 70 µM for those utilizing the RESA 10AA peptide. The RESA P2 peptide and RESA 10AA peptide were concentrated at 5-6 µM and 7-10 µM respectively. Fab (syringe) was titrated into the cell (peptide) at 25°C using a protocol involving 19 injections each at a volume of 2.0 µL. The curves were fitted to a 2:1 or 1:1 binding model using the MicroCal ITC Origin 7.0 Analysis Software.

Size-Exclusion Chromatography-Multi-Angle Light Scattering (SEC-MALS).

SEC-MALS experiments were performed at 4°C using a Superdex 200 Increase 10/300 GL (Cytiva #GE17-5175-01) column. RESA P2 peptide was incubated with B1E11K Fab at a 1:6 molar ratio for 30 minutes prior to loading onto the Superdex 200 column. The column was set up onto an Agilent Technologies 1260 Infinity II HPLC coupled with a MiniDawn Treos MALS detector

(Wyatt), Quasielastic light scattering (QELS) detector (Wyatt), and Optilab T-reX refractive index (RI) detector (Wyatt). Data processing was performed using the ASTRA software (Wyatt).

Negative Stain Electron Microscopy (nsEM) and Image Processing.

Fractions of the first peak of the SEC-MALS experiments containing the 2:1 B1E11K:RESA P2 complex were used to make nsEM grids. 50 µg/mL of the complex was deposited onto homemade carbon film-coated grids (previously glow-discharged in air for 15s) and stained with 2% uranyl formate. Data was collected onto a Hitachi HT7800 microscope paired with an EMSIS Xarosa 20 Megapixel CMOS camera. Micrographs were taken with the microscope operating at 120 kV at 80,000x magnification with a pixel size of 1.83 Å/px. Image processing, particle picking, extractions, 2D classifications, and 3D reconstructions were done in cryoSPARC v2 (79).

X-Ray Crystallography and Structural Determination.

The RESA P2 peptide was incubated with B1E11K Fab at a 1:5 molar ratio for 30 minutes prior to loading onto a Superdex 200 column Increase 10/300 GL column. Fractions containing the complex were pooled and concentrated at 8.6 mg/mL. A seed stock prepared from a previous crystallization trial was used for seeding. The stock was prepared from condition G9 of a JCSG Top96 screen (0.2M (NH4)2SO4 25% [w/v] PEG4000, and 0.1M sodium acetate [pH 4.6]). The complex, reservoir solution, and seed stock were mixed at a 3:4:1 volumetric ratio into an optimization tray derived from condition G9 of the JCSG Top96 screen. Crystals grew within 6 hours in a reservoir condition consisting of (0.1M NH4)2SO4 25% (w/v) PEG4000, and 0.1M sodium acetate (pH 5.2). Crystals were cryo-protected with 15% ethylene glycol (v/v) before being flash-frozen in liquid nitrogen. Data collection was performed at the 23-ID-B beamline at the Argonne National Laboratory Advanced Photon Source. Datasets were initially processed using autoproc (80) and further optimized using xdsgui (81). Molecular replacement was performed using PhaserMR (82) followed by multiple rounds of refinement using phenix.refine (83) and Coot (84). Inter- and intra-molecular contacts were determined using PISA (85) and manual inspection. Structural figures were generated using UCSF ChimeraX (86) (87).

Acknowledgements:

We thank A. Guarino for her support to antibody production, N. Thielens for her input during the course of this work, Y. Couté for the proteomics analysis, J-B. Reiser for the preliminary BLI experiments, L. Chaperot for providing CD40L expressing fibroblasts, E. Thai and D. Ivanochko for their contributions to X-ray data collection and structure determination, K. Teelen for assistance with ELISAs, M. van de Vegte-Bolmer and R. Stoter for parasite culture, G.J. van Gemert and L. Pelser and A. Pouwelsen and J. Kuhnen and J. Klaassen and S. Mulder for mosquito rearing and dissection, and K. Koolen for support with ELISA and gamete binding experiments. Furthermore, we would like to thank Jessica Chichester (Fraunhofer) for providing Pfs230CMB. This work was supported in part by the Bill & Melinda Gates Foundation (OPP1108403). This work was also undertaken, in part, thanks to funding from the Canadian Institutes for Health Research and was supported by the CIFAR Azrieli Global Scholar program (JPJ), the Ontario Early Researcher Award program (JPJ), and the Canada Research Chair program (JPJ). RY was supported by a Canada Graduate Scholarship - Master's (CGS-M). WS is supported by a Wellcome Trust Fellowship (218676/Z/19/Z). MMJ is supported by a Vidi grant from the Netherlands Organisation for Scientific Research (Vidi fellowship number 192.061). The proteomic experiments were partially supported by ANR grant ProFI (Proteomics French Infrastructure, ANR-10-INBS-08) and GRAL, a program from the Chemistry Biology Health (CBH) Graduate School of University Grenoble Alpes (ANR-17-EURE-0003). This work used the

platforms of the Grenoble Instruct-ERIC center (ISBG ; UAR 3518 CNRS-CEA-UGA-EMBL) within the Grenoble Partnership for Structural Biology (PSB), supported by FRISBI (ANR-10-INBS-0005-02) and GRAL, financed within the University Grenoble Alpes graduate school (Ecoles Universitaires de Recherche) CBH-EUR-GS (ANR-17-EURE-0003). Molecular graphics were generated using UCSF ChimeraX, developed by the Resource for Biocomputing, Visualization, and Informatics (University of California, San Francisco) with support from the National Institutes of Health (R01-GM129325) and the Office of Cyber Infrastructure and Computational Biology, National Institute of Allergy and Infectious Diseases.The BLI, ITC and SEC-MALS instruments were accessed at the Structural and Biophysical Core Facility, The Hospital for Sick Children, and EM data was collected at the Nanoscale Biomedical Imaging Facility, The Hospital for Sick Children, supported by the Canada Foundation for Innovation and Ontario Research Fund. X-ray diffraction experiments were in part performed using beamlines 23-ID-B at GM/CA@APS, which has been funded by the National Cancer Institute (ACB-12002) and the National Institute of General Medical Sciences (AGM-12006, P30GM138396). This research used resources of the Advanced Photon Source, a U.S. Department of Energy (DOE) Office of Science User Facility operated for the DOE Office of Science by Argonne National Laboratory under Contract No. DE-AC02-06CH11357. The Eiger 16M detector at GM/CA-XSD was funded NIH grant S10 OD012289. X-ray diffraction experiments were also performed using beamline AMX-17-ID-1 at the National Synchrotron Light Source II, a U.S. Department of Energy (DOE) Office of Science User Facility operated for the DOE Office of Science by Brookhaven National Laboratory under Contract No. DE-SC0012704. The Center for BioMolecular Structure (CBMS) is primarily supported by the National Institutes of Health, National Institute of General Medical Sciences (NIGMS) through a Center Core P30 Grant (P30GM133893), and by the DOE Office of Biological and Environmental Research (KP1607011). X-ray diffraction experiments were also performed using beamline CMCF-ID at the Canadian Light Source, a national research facility of the University of Saskatchewan, which is supported by the Canada Foundation for Innovation (CFI), the Natural Sciences and Engineering Research Council (NSERC), the National Research Council (NRC), the Canadian Institutes of Health Research (CIHR), the Government of Saskatchewan, and the University of Saskatchewan.

References:

1. World malaria report 2021.
2. Wicht KJ, Mok S, Fidock DA. Molecular Mechanisms of Drug Resistance in Plasmodium falciparum Malaria. Vol. 74, Annual Review of Microbiology. Annual Reviews Inc.; 2020. p. 431–54.
3. Florens L, Washburn MP, Dale Raine J, Anthony RM, Graingerk M, David Haynes J, et al. A proteomic view of the Plasmodium falciparum life cycle [Internet]. 2002. Available from: www.nature.com/nature
4. Cowman AF, Healer J, Marapana D, Marsh K. Malaria: Biology and Disease. Cell [Internet]. 2016;167(3):610–24. Available from: http://dx.doi.org/10.1016/j.cell.2016.07.055
5. Rosenberg R. Malaria: some considerations regarding parasite productivity. Trends Parasitol. 2008 Nov;24(11):487–91.
6. Laurens MB. RTS,S/AS01 vaccine (Mosquirix^{TM}): an overview. Hum Vaccin Immunother. 2019;
7. Datoo MS, Dicko A, Tinto H, Ouédraogo JB, Olotu A, Beaumont E, et al. A phase III randomised controlled trial evaluating the malaria vaccine candidate R21/Matrix-M^{TM} in African children [Internet]. Available from: https://ssrn.com/abstract=4584076
8. Cerami C, Frevert U, Sinnis P, Takacs B, Clavijo P, Santos MJ, et al. The Basolateral Domain of the Hepatocyte Plasma Membrane Bears Receptors for the Circumsporozoite Protein of Plasmodium falciparum Sporozoites. Vol. 70, Cell. 1992.
9. Frevert U, Sinnis P, Cerami C, Shrefl W, Takacs B, Nussenzweig V. Malaria Circumsporozoite Protein Binds to Heparan Sulfate Proteoglycans Associated with the Surface Membrane of Hepatocytes [Internet]. Available from: http://rupress.org/jem/article-pdf/177/5/1287/1674538/1287.pdf
10. Ménard Robert, Sultan Ali, Cortes Claudio, Altszuler Rita, van Dijk Mélissa, Janse Chris, et al. Circumsporozoite protein is required for development of malaria sporozoites in mosquitoes.
11. Kucharska I, Thai E, Srivastava A, Rubinstein JL, Pomès R, Julien JP. Structural ordering of the plasmodium berghei circumsporozoite protein repeats by inhibitory antibody 3d11. Elife. 2020 Oct 1;9:1–25.
12. Imkeller K, Scally SW, Bosch A, Martí GP, Costa G, Triller G, et al. Antihomotypic affinity maturation improves human B cell responses against a repetitive epitope [Internet]. Available from: www.imgt.org/genedb/.
13. Martin GM, Torres JL, Pholcharee T, Oyen D, Flores-Garcia Y, Gibson G, et al. Affinity-matured homotypic interactions induce spectrum of PfCSP structures that influence protection from malaria infection. Nat Commun. 2023 Dec 1;14(1).
14. Pholcharee T, Oyen D, Flores-Garcia Y, Gonzalez-Paez G, Han Z, Williams KL, et al. Structural and biophysical correlation of anti-NANP antibodies with in vivo protection against P. falciparum. Nat Commun. 2021 Dec 1;12(1).
15. Oyen D, Torres JL, Cottrell CA, Richter King C, Wilson IA, Ward AB. Cryo-EM structure of P. falciparum circumsporozoite protein with a vaccine-elicited antibody is stabilized by somatically mutated inter-Fab contacts. Vol. 4, Sci. Adv. 2018.

16. Martin GM, Fernández-Quintero ML, Lee WH, Pholcharee T, Eshun-Wilson L, Liedl KR, et al. Structural basis of epitope selectivity and potent protection from malaria by PfCSP antibody L9. Nat Commun. 2023 Dec 1;14(1).
17. Kucharska I, Hossain L, Ivanochko D, Yang Q, Rubinstein JL, Pomès R, et al. Structural basis of Plasmodium vivax inhibition by antibodies binding to the circumsporozoite protein repeats. Elife. 2022 Jan 1;11.
18. Murugan R, Scally SW, Costa G, Mustafa G, Thai E, Decker T, et al. Evolution of protective human antibodies against Plasmodium falciparum circumsporozoite protein repeat motifs. Nature Medicine 2020 26:7 [Internet]. 2020 May 25 [cited 2023 Oct 22];26(7):1135–45. Available from: https://www.nature.com/articles/s41591-020-0881-9
19. Tripathi P, Bender MF, Lei H, Da Silva Pereira L, Shen CH, Bonilla B, et al. Cryo-EM structures of anti-malarial antibody L9 with circumsporozoite protein reveal trimeric L9 association and complete 27-residue epitope. Structure [Internet]. 2023 Apr 6 [cited 2023 Oct 22];31(4):480-491.e4. Available from: http://www.cell.com/article/S0969212623000436/fulltext
20. Efficacy and safety of RTS,S/AS01 malaria vaccine with or without a booster dose in infants and children in Africa: Final results of a phase 3, individually randomised, controlled trial. The Lancet. 2015 Jul 4;386(9988):31–45.
21. Wadman M. First malaria vaccine slashes childhood deaths. Science (1979) [Internet]. 2023 Oct 27;382(6669):357–357. Available from: https://www.science.org/doi/10.1126/science.adl5521
22. Golumbeanu M, Yang GJ, Camponovo F, Stuckey EM, Hamon N, Mondy M, et al. Leveraging mathematical models of disease dynamics and machine learning to improve development of novel malaria interventions. Infect Dis Poverty. 2022 Dec 1;11(1).
23. Stone WJR, Dantzler KW, Nilsson SK, Drakeley CJ, Marti M, Bousema T, et al. Naturally acquired immunity to sexual stage P. Falciparum parasites. Vol. 143, Parasitology. Cambridge University Press; 2016. p. 187–98.
24. Duffy PE. Transmission-Blocking Vaccines: Harnessing Herd Immunity for Malaria Elimination. Vol. 20, Expert Review of Vaccines. Taylor and Francis Ltd.; 2021. p. 185–98.
25. Roeffen W, Teelen K, Van As J, Vd Vegte-Bolmer M, Eling W, Sauerwein R. Plasmodium falciparum: Production and characterization of rat monoclonal antibodies specific for the sexual-stage Pfs48/45 antigen. Exp Parasitol. 2001;97(1):45–9.
26. Ivanochko D, Fabra-García A, Teelen K, van de Vegte-Bolmer M, van Gemert GJ, Newton J, et al. Potent transmission-blocking monoclonal antibodies from naturally exposed individuals target a conserved epitope on Plasmodium falciparum Pfs230. Immunity. 2023 Feb 14;56(2):420-432.e7.
27. Fabra-García A, Hailemariam S, de Jong RM, Janssen K, Teelen K, van de Vegte-Bolmer M, et al. Highly potent, naturally acquired human monoclonal antibodies against Pfs48/45 block Plasmodium falciparum transmission to mosquitoes. Immunity. 2023 Feb 14;56(2):406-419.e7.

28. Kundu P, Semesi A, Jore MM, Morin MJ, Price VL, Liang A, et al. Structural delineation of potent transmission-blocking epitope I on malaria antigen Pfs48/45. Nat Commun. 2018 Dec 1;9(1).
29. Stone WJR, Campo JJ, Ouédraogo AL, Meerstein-Kessel L, Morlais I, Da D, et al. Unravelling the immune signature of Plasmodium falciparum transmission-reducing immunity. Nat Commun. 2018 Dec 1;9(1).
30. Coelho CH, Tang WK, Burkhardt M, Galson JD, Muratova O, Salinas ND, et al. A human monoclonal antibody blocks malaria transmission and defines a highly conserved neutralizing epitope on gametes. Nat Commun. 2021 Dec 1;12(1).
31. Tang WK, Coelho CH, Miura K, Nguemwo Tentokam BC, Salinas ND, Narum DL, et al. A human antibody epitope map of Pfs230D1 derived from analysis of individuals vaccinated with a malaria transmission-blocking vaccine. Immunity. 2023 Feb 14;56(2):433-443.e5.
32. Ko KT, Lennartz F, Mekhaiel D, Guloglu B, Marini A, Deuker DJ, et al. Structure of the malaria vaccine candidate Pfs48/45 and its recognition by transmission blocking antibodies. Nat Commun. 2022 Dec 1;13(1).
33. Lennartz F, Brod F, Dabbs R, Miura K, Mekhaiel D, Marini A, et al. Structural basis for recognition of the malaria vaccine candidate Pfs48/45 by a transmission blocking antibody. Nat Commun. 2018 Dec 1;9(1).
34. Singh K, Burkhardt M, Nakuchima S, Herrera R, Muratova O, Gittis AG, et al. Structure and function of a malaria transmission blocking vaccine targeting Pfs230 and Pfs230-Pfs48/45 proteins. Commun Biol. 2020 Dec 1;3(1).
35. Brooks SR, Williamson KC. Proteolysis of Plasmodium falciparum surface antigen, Pfs230, during gametogenesis [Internet]. Vol. 106, Molecular and Biochemical Parasitology. 2000. Available from: www.elsevier.com/locate/parasitology
36. Tiller T, Meffre E, Yurasov S, Tsuiji M, Nussenzweig MC, Wardemann H. Efficient generation of monoclonal antibodies from single human B cells by single cell RT-PCR and expression vector cloning. J Immunol Methods. 2008 Jan 1;329(1–2):112–24.
37. Kundu P, Semesi A, Jore MM, Morin MJ, Price VL, Liang A, et al. Structural delineation of potent transmission-blocking epitope I on malaria antigen Pfs48/45. Nat Commun [Internet]. 2018 Dec 26 [cited 2019 Jan 14];9(1):4458. Available from: http://www.nature.com/articles/s41467-018-06742-9
38. Coelho CH, Tang WK, Burkhardt M, Galson JD, Muratova O, Salinas ND, et al. A human monoclonal antibody blocks malaria transmission and defines a highly conserved neutralizing epitope on gametes. Nat Commun [Internet]. 2021;1–12. Available from: http://dx.doi.org/10.1038/s41467-021-21955-1
39. Hou N, Jiang N, Ma Y, Zou Y, Piao X, Liu S, et al. Low-Complexity Repetitive Epitopes of Plasmodium falciparum Are Decoys for Humoural Immune Responses. Front Immunol. 2020 Apr 15;11.
40. Raghavan M, Kalantar KL, Duarte E, Teyssier N, Takahashi S, Kung AF, et al. Proteome-wide antigenic profiling in Ugandan cohorts identifies associations between age, exposure intensity, and responses to repeat-containing antigens in Plasmodium falciparum. Elife. 2023 Feb 1;12.

41. Cardoso RMF, Zwick MB, Stanfield RL, Kunert R, Binley JM, Katinger H, et al. Broadly neutralizing anti-HIV antibody 4E10 recognizes a helical conformation of a highly conserved fusion-associated motif in gp41. Immunity. 2005;22(2):163–73.
42. Heger A, Holm L. Rapid Automatic Detection and Alignment of Repeats in Protein Sequences. 2000.
43. Williamsona· KC, Fujiokab H, Aikawab M, Kaslowc DC. Stage-specific processing of Pfs230, a Plasmodium falciparum transmission-blocking vaccine candidate. Vol. 78, Molecular and Biochemical Parasitology. 1996.
44. De Jong RM. Towards efficacious transmission blocking malaria vaccines The long and winding path.. Towards efficacious transmission blocking malaria vaccines. 2023.
45. Ye J, Ma N, Madden TL, Ostell JM. IgBLAST: an immunoglobulin variable domain sequence analysis tool. Nucleic Acids Res. 2013;41(Web Server issue).
46. Miura K, Takashima E, Pham TP, Deng B, Zhou L, Huang WC, et al. Elucidating functional epitopes within the N-terminal region of malaria transmission blocking vaccine antigen Pfs230. NPJ Vaccines. 2022 Dec 1;7(1).
47. Simon N, Kuehn A, Williamson KC, Pradel G. Adhesion protein complexes of malaria gametocytes assemble following parasite transmission to the mosquito. Parasitol Int. 2016 Feb 1;65(1):27–30.
48. Feng Z, Hoffmann KN, Nussenzweig RS, Tsuji M, Fujioka H, Aikawa M, et al. Pfs2400 Can Mediate Antibody-dependent Malaria Transmission Inhibition and May Be the Plasmodium Falciparum 11.1 Gene Product [Internet]. Available from: http://rupress.org/jem/article-pdf/177/2/273/1103419/273.pdf
49. Scherf A, Carter' R, Petersen2 C, Alano3 P, Nelson2 R, Aikawa4 M, et al. Gene inactivation of Pf 11-1 of Plasmodium falciparum by chromosome breakage and healing: identification of a gametocyte-specific protein with a potential role in gametogenesis. Vol. 1, The EMBO Journal. 1992.
50. Masuda A, Zavala F, Nussenzweig V, Nussenzweig RS. Monoclonal anti-gametocyte antibodies identify an antigen present in all blood stages of Plasmodium faIciparum. Vol. 19, Molecular and Biochemical Parasitology. 1986.
51. Udomsangpetch Rachanee, Lundgren Katarina, Berzins Klaus, Wahlin Birgitta, Perlmann Hedvig, Troye-Blomberg Marita, et al. Human monoclonal antibodies to Pf 155 a major antigen of malaria parasite Plasmodium falciparum.
52. Ahlborg N, Berzins K, Perlmann P. Definition of the epitope recognized by the Plasmodiumfalciparum-reactive human monoclonal antibody 33G2. Vol. 46, Molecular and Biochemical Parasitology. 1991.
53. Udomsangpetch Rachanee, Carlsson Jan, Wahlin Birgitta, Holmquist Goran, Ozaki Luiz, Scherf Arthur, et al. Reactivity of the human monoclonal antibody 33G2 with repeated sequences of three distinct Plasmodium falciparum antigens [Internet]. 2018. Available from: http://www.jimmunol.org/content/142/10/3620
54. Kucharska I, Binter Š, Murugan R, Scally SW, Ludwig J, Prieto K, et al. High-density binding to Plasmodium falciparum circumsporozoite protein repeats by inhibitory antibody elicited in mouse with human immunoglobulin repertoire. PLoS Pathog. 2022 Nov 1;18(11).
55. Clutterbuck EA, Lazarus R, Yu LM, Bowman J, Bateman EAL, Diggle L, et al. Pneumococcal conjugate and plain polysaccharide vaccines have divergent effects

on antigen-specific B cells. Journal of Infectious Diseases. 2012 May 1;205(9):1408–16.

56. Wahl I, Wardemann H. How to induce protective humoral immunity against Plasmodium falciparum circumsporozoite protein. Vol. 219, Journal of Experimental Medicine. Rockefeller University Press; 2022.

57. Murugan R, Scally SW, Costa G, Mustafa G, Thai E, Decker T, et al. Evolution of protective human antibodies against Plasmodium falciparum circumsporozoite protein repeat motifs. Nat Med. 2020 Jul 1;26(7):1135–45.

58. Ludwig J, Scally SW, Costa G, Hoffmann S, Murugan R, Lossin J, et al. Glycosylated nanoparticle-based PfCSP vaccine confers long-lasting antibody responses and sterile protection in mouse malaria model. NPJ Vaccines. 2023 Dec 1;8(1).

59. Thai E, Murugan R, Binter Š, Burn Aschner C, Prieto K, Kassardjian A, et al. Molecular determinants of cross-reactivity and potency by VH3-33 antibodies against the Plasmodium falciparum circumsporozoite protein. Cell Rep [Internet]. 2023 Nov;42(11):113330. Available from: https://linkinghub.elsevier.com/retrieve/pii/S2211124723013426

60. Chatterjee D, Lewis FJ, Sutton HJ, Kaczmarski JA, Gao X, Cai Y, et al. Avid binding by B cells to the Plasmodium circumsporozoite protein repeat suppresses responses to protective subdominant epitopes. Cell Rep. 2021 Apr 13;35(2).

61. Chatterjee D, Cockburn IA. The challenges of a circumsporozoite protein-based malaria vaccine. Expert Rev Vaccines [Internet]. 2021 Feb 1 [cited 2023 Oct 30];20(2):113–25. Available from: https://www.tandfonline.com/doi/abs/10.1080/14760584.2021.1874924

62. McNamara HA, Idris AH, Sutton HJ, Vistein R, Flynn BJ, Cai Y, et al. Antibody Feedback Limits the Expansion of B Cell Responses to Malaria Vaccination but Drives Diversification of the Humoral Response. Cell Host Microbe. 2020 Oct 7;28(4):572-585.e7.

63. Nahrendorf W, Scholzen A, Sauerwein RW, Langhorne J. Cross-stage immunity for malaria vaccine development. Vaccine. 2015 Dec 22;33(52):7513–7.

64. Julien JP, Wardemann H. Antibodies against Plasmodium falciparum malaria at the molecular level. Vol. 19, Nature Reviews Immunology. Nature Research; 2019. p. 761–75.

65. Riley EM, Allen SJ, Troye-Blomberg M, Bennett S, Perlmann H, Andersson G, et al. Association between immune recognition of the malaria vaccine candidate antigen Pf155/RESA and resistance to clinical disease: a prospective study in a malaria-endemic region of West Africa. Trans R Soc Trop Med Hyg [Internet]. 1991 Jul 1 [cited 2023 Oct 22];85(4):436–43. Available from: https://dx.doi.org/10.1016/0035-9203(91)90207-F

66. Petersen E, Høgh B, Marbiah NT, Perlmann H, Willcox M, Dolopaie E, et al. A longitudinal study of antibodies to the Plasmodium falciparum antigen Pf155/RESA and immunity to malaria infection in adult Liberians. Trans R Soc Trop Med Hyg [Internet]. 1990 Jun 1 [cited 2023 Oct 22];84(3):339–45. Available from: https://dx.doi.org/10.1016/0035-9203(90)90307-Z

67. Berzins K, Perlmann H, Wahlin B, Ekre HP, Hogh B, Petersen E, et al. Passive Immunization of Aotus Monkeys with Human Antibodies to the Plasmodium

falciparum Antigen Pfl55/RESA [Internet]. Vol. 59, INFECTION AND IMMUNITY. 1991. Available from: https://journals.asm.org/journal/iai

68. Garrone P, Neidhardt EM, Garcia E, Galibert L, Van Kooten C, Banchereau J. Fas Ligation Induces Apoptosis of CD40-activated Human B Lymphocytes.

69. Lefranc MP, Giudicelli V, Duroux P, Jabado-Michaloud J, Folch G, Aouinti S, et al. IMGT R, the international ImMunoGeneTics information system R 25 years on. Nucleic Acids Res. 2015 Jan 28;43(D1):D413–22.

70. Van Dijk MR, Janse CJ, Thompson J, Waters AP, Braks JAM, Dodemont HJ, et al. A Central Role for P48/45 in Malaria Parasite Male Gamete Fertility The central role of zygote formation in the life cycle and transmission of the parasite makes gametes and. Vol. 104, Cell. 2001.

71. KUMAR Nirbhay. Target antigens of malaria transmission blocking immunity exist as a stable membrane bound complex. Vol. 9, Parasite Immunology. 1987.

72. Farrance CE, Rhee A, Jones RM, Musiychuk K, Shamloul M, Sharma S, et al. A plant-produced Pfs230 vaccine candidate blocks transmission of Plasmodium falciparum. Clinical and Vaccine Immunology. 2011 Aug;18(8):1351–7.

73. Ponnudurai T, Lensen AHW, Van Gemert GJA, Bensink MPE, Bolmer M, Meuwissen JHET. Infectivity of cultured Plasmodium falciparum gametocytes to mosquitoes. Parasitology. 1989;98(2):165–73.

74. de Jong RM, Singh SK, Teelen K, van de Vegte-Bolmer M, van Gemert GJ, Stone WJR, et al. Heterologous Expression and Evaluation of Novel Plasmodium falciparum Transmission Blocking Vaccine Candidates. Front Immunol. 2022 Jun 23;13.

75. de Jong RM, Alkema M, Oulton T, Dumont E, Teelen K, Nakajima R, et al. The acquisition of humoral immune responses targeting Plasmodium falciparum sexual stages in controlled human malaria infections. Front Immunol. 2022 Jul 18;13.

76. Meerstein-Kessel L, Van Der Lee R, Stone W, Lanke K, Baker DA, Alano P, et al. Probabilistic data integration identifies reliable gametocyte-specific proteins and transcripts in malaria parasites. Sci Rep. 2018 Dec 1;8(1).

77. Staples TL. Expansion and evolution of the R programming language. R Soc Open Sci. 2023 Apr 12;10(4).

78. Ritchie ME, Phipson B, Wu D, Hu Y, Law CW, Shi W, et al. Limma powers differential expression analyses for RNA-sequencing and microarray studies. Nucleic Acids Res. 2015 Jan 6;43(7):e47.

79. Punjani A, Rubinstein JL, Fleet DJ, Brubaker MA. cryoSPARC: algorithms for rapid unsupervised cryo-EM structure determination. Nature Methods 2017 14:3 [Internet]. 2017 Feb 6 [cited 2023 Oct 22];14(3):290–6. Available from: https://www.nature.com/articles/nmeth.4169

80. Vonrhein C, Flensburg C, Keller P, Sharff A, Smart O, Paciorek W, et al. Data processing and analysis with the autoPROC toolbox. Acta Crystallogr D Biol Crystallogr. 2011 Apr;67(4):293–302.

81. Kabsch W. *XDS*. Acta Crystallogr D Biol Crystallogr [Internet]. 2010 Feb 1;66(2):125–32. Available from: https://scripts.iucr.org/cgi-bin/paper?S0907444909047337

82. McCoy AJ, Grosse-Kunstleve RW, Adams PD, Winn MD, Storoni LC, Read RJ. Phaser crystallographic software. J Appl Crystallogr. 2007 Jul 13;40(4):658–74.

83. Liebschner D, Afonine P V., Baker ML, Bunkoczi G, Chen VB, Croll TI, et al. Macromolecular structure determination using X-rays, neutrons and electrons: Recent developments in Phenix. Acta Crystallogr D Struct Biol. 2019 Oct 1;75:861–77.
84. Emsley P, Lohkamp B, Scott WG, Cowtan K. Features and development of Coot. Acta Crystallogr D Biol Crystallogr. 2010;66(4):486–501.
85. Krissinel E, Henrick K. Inference of Macromolecular Assemblies from Crystalline State. J Mol Biol. 2007 Sep 21;372(3):774–97.
86. Goddard TD, Huang CC, Meng EC, Pettersen EF, Couch GS, Morris JH, et al. UCSF ChimeraX: Meeting modern challenges in visualization and analysis. Protein Science. 2018 Jan 1;27(1):14–25.
87. Pettersen EF, Goddard TD, Huang CC, Meng EC, Couch GS, Croll TI, et al. UCSF ChimeraX: Structure visualization for researchers, educators, and developers. Protein Science. 2021 Jan 1;30(1):70–82.

Figures and Tables:

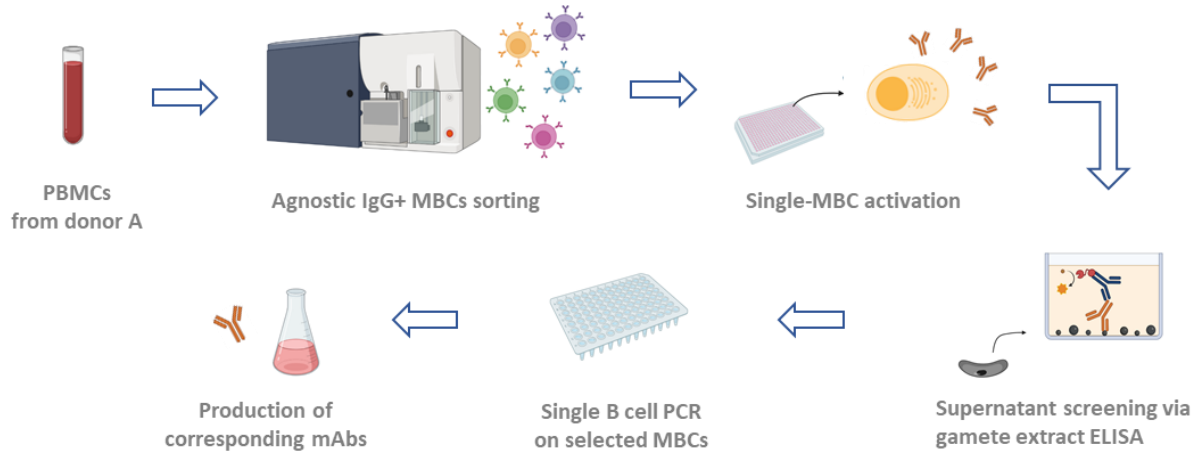

Figure 1: General workflow. IgG+ memory B cells from Donor A were sorted individually regardless of their specificity, at one cell per well. Cells were further cultured in activation medium with CD40L-expressing feeder cells and cytokines to induce antibody secretion. Supernatants were tested for antibody binding to the sexual stage of the parasite through screening using a gamete extract ELISA. Memory B cells from wells displaying reactivity were selected for Ig genes amplification, followed by cloning and production of the corresponding antibody.

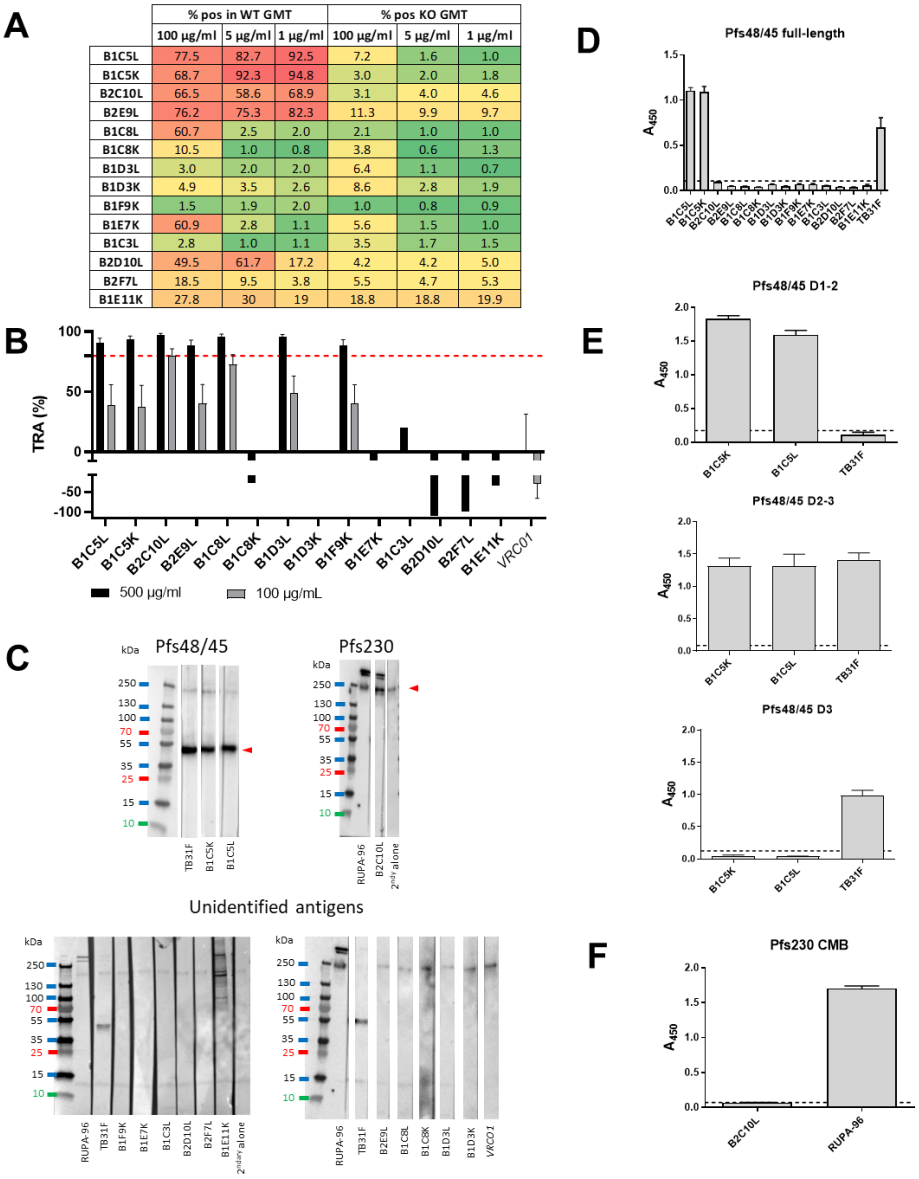

	% pos in WT GMT			% pos KO GMT		
	100 µg/ml	5 µg/ml	1 µg/ml	100 µg/ml	5 µg/ml	1 µg/ml
B1C5L	77.5	82.7	92.5	7.2	1.6	1.0
B1C5K	68.7	92.3	94.8	3.0	2.0	1.8
B2C10L	66.5	58.6	68.9	3.1	4.0	4.6
B2E9L	76.2	75.3	82.3	11.3	9.9	9.7
B1C8L	60.7	2.5	2.0	2.1	1.0	1.0
B1C8K	10.5	1.0	0.8	3.8	0.6	1.3
B1D3L	3.0	2.0	2.0	6.4	1.1	0.7
B1D3K	4.9	3.5	2.6	8.6	2.8	1.9
B1F9K	1.5	1.9	2.0	1.0	0.8	0.9
B1E7K	60.9	2.8	1.1	5.6	1.5	1.0
B1C3L	2.8	1.0	1.1	3.5	1.7	1.5
B2D10L	49.5	61.7	17.2	4.2	4.2	5.0
B2F7L	18.5	9.5	3.8	5.5	4.7	5.3
B1E11K	27.8	30	19	18.8	18.8	19.9

Figure 2: Characterization of the panel of isolated monoclonal antibodies. (A) Percentage of binding to wild type (WT) and Pfs48/45 knock-out (KO) gametes in SIFA, in a heatmap format. The experiment was performed in duplicate and three different monoclonal antibody concentrations were tested (100 µg/ml, 5 µg/ml and 1µg/ml). GMT: gamete. (B) TRA of the mAb panel in SMFA: seven mAbs demonstrated TRA above 80% (red dotted line) when tested at 500 µg/ml in SMFA. For TRAbs, experiments were run in duplicates and bars are estimates of the mean and error bars represent the 95% confidence intervals. TRAbs were also tested at 100 µg/ml. (C) Reactivity of the monoclonal antibody panel against gametocyte extract in Western blot, in non-reducing conditions. Antibodies are classified depending on the antigen recognized: Pfs48/45, Pfs230, or no antigen identified. TB31F is an anti-Pfs 48/45 monoclonal antibody, RUPA-96 is an anti-Pfs230 monoclonal antibody, and VRCO1 is an anti-HIV monoclonal antibody (negative control). (D) Reactivity of the monoclonal antibody panel against full-length Pfs48/45 at 30 µg/ml in ELISA. (E) B1C5K and B1C5L binding to various Pfs48/45 domains in ELISA, at 10 µg/ml. (F) B2C10L binding to Pfs230 CMB domain in ELISA, at 10 µg/ml.

A

Peptide ID	Corresponding protein	Peptide position in the protein *Peptide length*	Normalised score	Corrected score
PF3D7_0220000	Liver Stage Antigen 3	67 to 822 *756*	6.253495	59988.5
PF3D7_0309100	OMD protein	Full length *187*	6.188559	57356
PF3D7_1149200	ring infected erythrocyte surface antigen 3 (RESA3)	65 to 587 *523*	6.193454	54235.5
PF3D7_0102200	ring infected erythrocyte surface antigen (RESA)	568 to 1085 (end) *518*	6.044558	53268
PF3D7_1127500	Protein disulfide isomerase	Full length *433*	5.913398	44843.5
PF3D7_1036300	Duffy binding like merozoite surface protein 2	423 to 762 *340*	5.433248	32032.5
PF3D7_0411700	conserved plasmodium protein	138	5.111879	25673.5
PF3D7_1038400	Pf 11.1	2980 to 3637 *658*	4.763914	21787
PF3D7_1149200	ring infected erythrocyte surface antigen 3	570 to 1090 *521*	4.723332	20946.5
PF3D7_0804500	uncharacterized protein	215	4.610963	19703
PF3D7_1038400	Pf 11.1	8737 to 9663 (end) *827*	3.986108	12776.5
PF3D7_1038400	Pf 11.1	7795 to 8628 *778*	3.757038	11117.5
PF3D7_0909000	uncharacterized protein	528	3.689088	10267
PF3D7_1038400	Pf 11.1	103 to 1024 *922*	3.242688	7017
PF3D7_0522400	uncharacterized protein	934	3.164308	6643.5

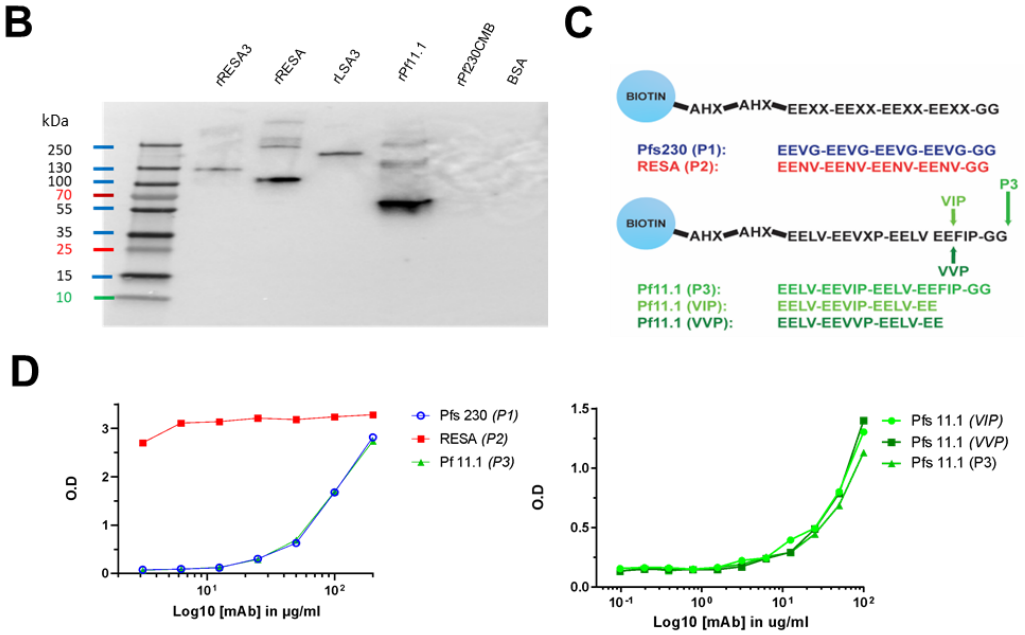

Figure 3: B1E11K binds repeat peptides. (A) B1E11K binding to recombinant fragments of Pf proteins displayed on a microarray. (B) B1E11K binding to several recombinant proteins in Western blot, in non-reducing conditions. (C) Sequences of the peptides tested for binding. Peptides were N-terminally linked to a biotin moiety using aminohexanoyl (Ahx) spacers. (D) B1E11K binding in ELISA to a panel of peptides.

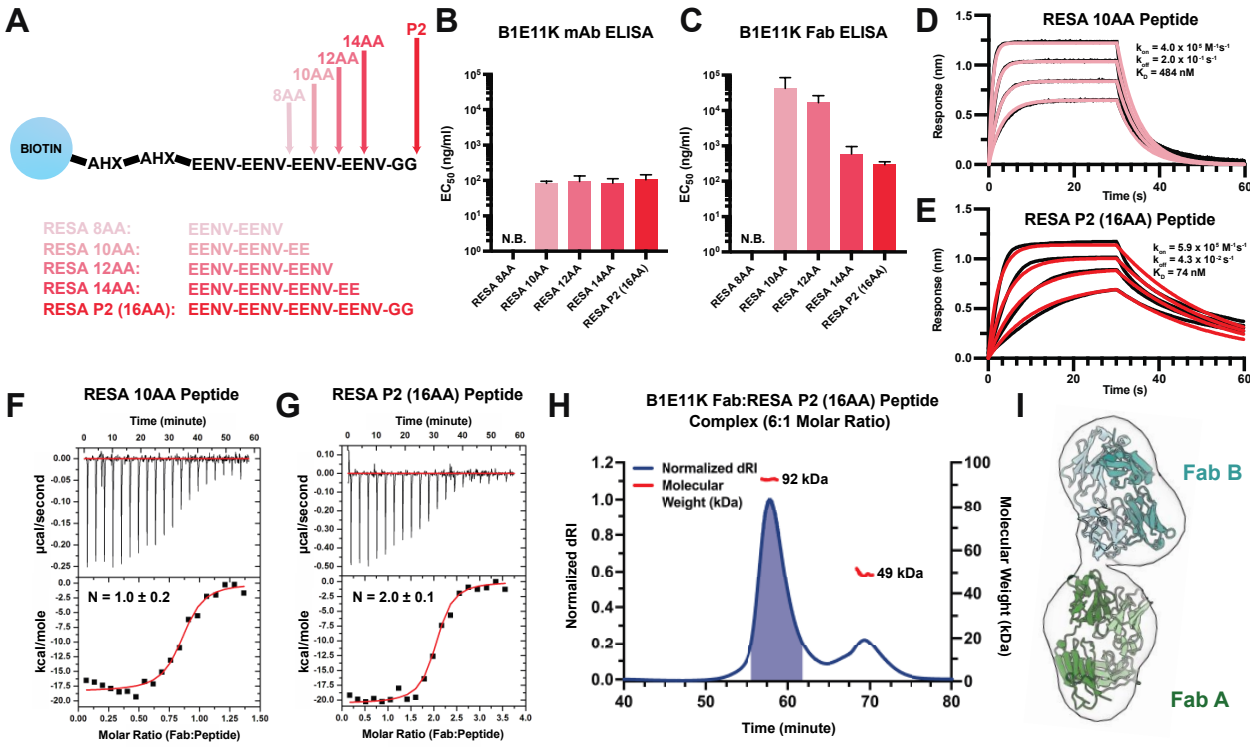

Figure 4: Binding Characteristics of RESA peptides to B1E11K. (A) Various peptides based on the EENV repeat region were designed and conjugated to a biotin-AHX-AHX moiety (AHX = ε-aminocaproic acid). EC_{50} values obtained from ELISA experiments utilizing various EENV repeat peptides with (B) B1E11K mAb or (C) B1E11K Fab. Error bars represent standard deviation. Biolayer interferometry experiments utilizing immobilized (D) RESA 10AA peptide or (E) RESA P2 (16AA) peptide dipped into B1E11K Fab. Representative isothermal titration calorimetry experiments in which B1E11K Fab was injected into (F) RESA 10AA peptide or (G) RESA P2 (16AA) peptide. (H) Size-exclusion chromatography coupled with multi-angle light scattering (SEC-MALS) of a solution of B1E11K Fab incubated with RESA P2 (16AA) peptide in a 6:1 molar ratio. The predicted molecular weight of the B1E11K Fab and RESA P2 peptide are 46.9 kDa and 2.5 kDa respectively. The shaded region indicates the fractions collected used for negative stain electron microscopy. (I) A nsEM map reconstruction which permits the fitting of two B1E11K Fabs (Fab A and Fab B).

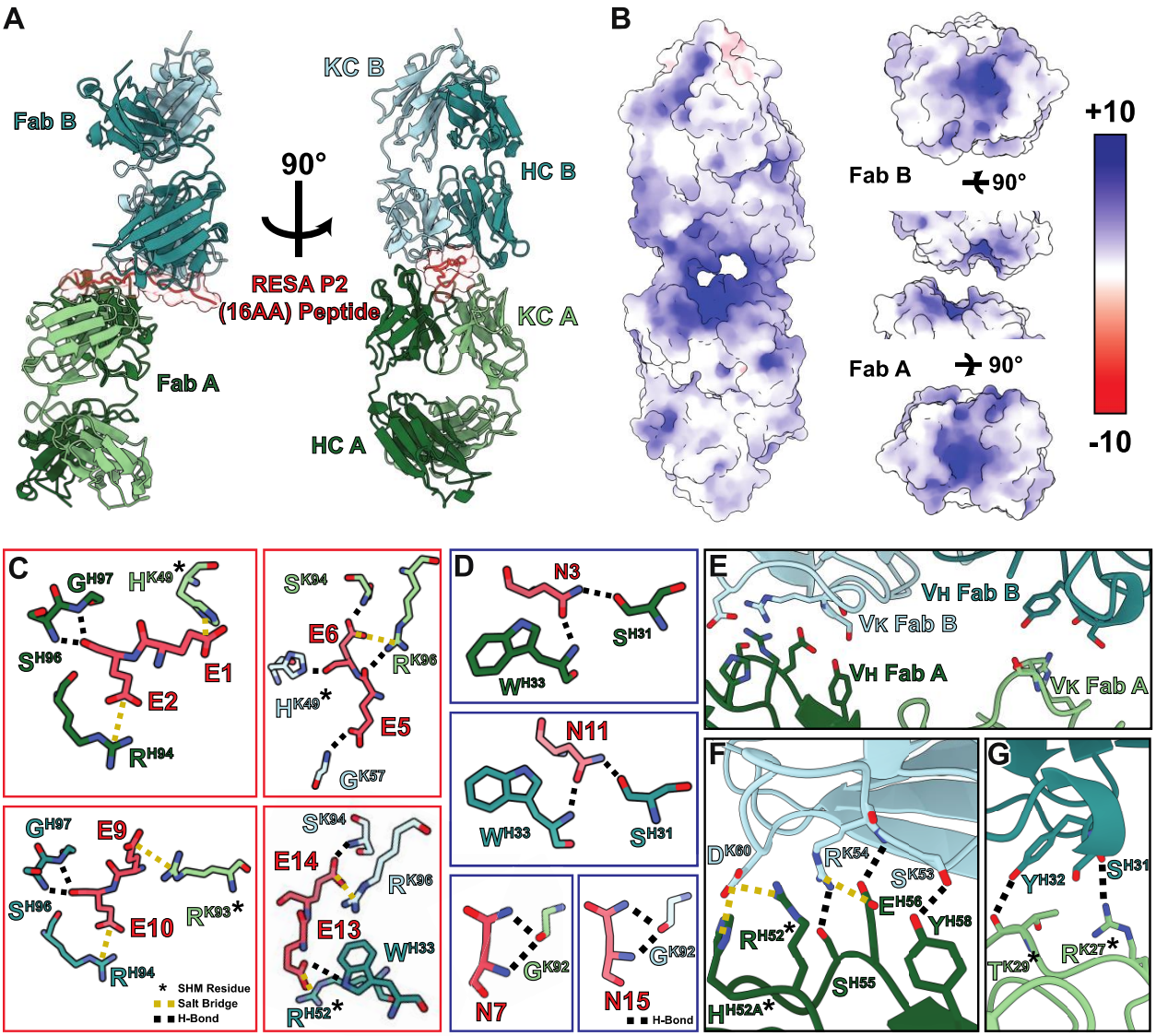

Figure 5: Structure of the B1E11K Fab and RESA P2 (16AA) peptide complex. (A) The overall architecture of the B1E11K:RESA P2 (16AA) peptide complex. (B) The electrostatic potential of the surface of the B1E11K Fabs. (C) Electrostatic interactions occurring with glutamate residues of the RESA P2 (16AA) peptide. Residues that have undergone somatic hypermutation (SHM) are marked with an asterisk. Salt bridges are shown as dashed yellow lines and hydrogen bonds as dashed black lines. (G) Hydrogen bonding interactions through the asparagine residues of the RESA P2 (16AA) peptide are shown as black dashed lines. (E) Variable heavy (V_H) and variable kappa (V_K) residues involved in homotypic interactions are shown as sticks. (F) The first interaction interface and (G) second interface. Residues that have undergone somatic hypermutation (SHM) are marked with an asterisk. Electrostatic interactions are presented as dashed lines and coloured as done previously.

Table 1: ITC thermodynamics and binding affinity of B1E11K Fab to RESA peptides.

	RESA 10AA peptide (n=2)	RESA P2 peptide (n=3)
N	1.0 ± 0.2	2.0 ± 0.1
K_D (nM)	77 ± 12	73 ± 20
ΔG (kJ/mole)	-62.1 ± 0.4	-61.9 ± 0.7
ΔH (kJ/mole)	-76.5 ± 0.5	-85.6 ± 0.4
-TΔS (kJ/mole)	14.3 ± 0.2	23.7 ± 0.8

Error reported as standard deviation.

Table 2: Crystallography statistics.

Crystal	**B1E11K:RESA P2 (16AA) peptide**
Beamline	APS-23-ID-B
Wavelength (Å)	1.0332
Space group	C 2 2 2_1
Cell dimensions	
a,b,c (Å)	78.7, 186.3, 131.5
α, β, γ (°)	90, 90, 90
Resolution (Å)[a]	40.0 - 2.53 (2.65 – 2.56)
No. molecules in ASU	1
No. of observations	236,070 (23,834)
No. unique observations	31,520 (3,067)
Multiplicity	7.5 (7.8)
R_{merge} (%)[b]	14.5 (222.8)
R_{pim} (%)[c]	5.7 (85.5)
<I/σI>	10.8 (1.0)
$CC_{1/2}$ (%)	99.7 (36.5)
Completeness (%)	99.8 (98.5)
Refinement Statistics	
Reflections used in refinement	31,512
Reflections used in R-free	1,575
Non-hydrogen atoms	6,781
Macromolecule	6,627
Water	130
Heteroatom	24
R_{work}[d] / R_{free}[e] (%)	21.5 / 24.5
Rms deviations from ideality	
Bond lengths (Å)	0.002
Bond angle (°)	0.48
Ramachandran plot	
Favoured regions (%)	96.0
Allowed regions (%)	3.8
B-factors (Å^2)	
Wilson B-factor	65.5
Average B-factors	89.8
Average macromolecule	90.3
Average Heteroatom	83.1
Average water molecule	61.0

[a]Values in parentheses refer to the highest resolution bin.

[b]$R_{merge} = \Sigma_{hkl} \Sigma_i | I_{hkl,i} - \langle I_{hkl} \rangle | / \Sigma_{hkl} \langle I_{hkl} \rangle$

[c]$R_{pim} = \Sigma_{hkl} [1/(N-1)]^{1/2} \Sigma i | I_{hkl,i} - \langle I_{hkl} \rangle | / \Sigma_{hkl} \langle I_{hkl} \rangle$

[d]$R_{work} = (\Sigma | |Fo| - |Fc| |) / (\Sigma | |F_o|)$ - for all data except as indicated in footnote e.

[e]5% of data were used for the R_{free} calculation.